Climate
of the Past

Open Access

Limited response of peatland CH$_4$ emissions to abrupt Atlantic Ocean circulation changes in glacial climates

P. O. Hopcroft[1], P. J. Valdes[1], R. Wania[*], and D. J. Beerling[2]

[1]Bristol Research Initiative for the Dynamic Global Environment (BRIDGE), School of Geographical Sciences, University of Bristol, Bristol, BS8 1SS, UK
[2]Department of Animal and Plant Sciences, University of Sheffield, Sheffield, S10 2TN, UK
[*]formerly at: Institut des Sciences de l'Evolution, CNRS – UMR5554, Universite Montpellier 2, Place Eugene Bataillon, 34090 Montpellier, France

Correspondence to: P. O. Hopcroft (peter.hopcroft@bris.ac.uk)

Abstract. Ice-core records show that abrupt Dansgaard–Oeschger (D–O) climatic warming events of the last glacial period were accompanied by large increases in the atmospheric CH$_4$ concentration (up to 200 ppbv). These abrupt changes are generally regarded as arising from the effects of changes in the Atlantic Ocean meridional overturning circulation and the resultant climatic impact on natural CH$_4$ sources, in particular wetlands. We use two different ecosystem models of wetland CH$_4$ emissions to simulate northern CH$_4$ sources forced with coupled general circulation model simulations of five different time periods during the last glacial to investigate the potential influence of abrupt ocean circulation changes on atmospheric CH$_4$ levels during D–O events. The simulated warming over Greenland of 7–9 °C in the different time periods is at the lower end of the range of 11–15 °C derived from ice cores, but is associated with strong impacts on the hydrological cycle, especially over the North Atlantic and Europe during winter. We find that although the sensitivity of CH$_4$ emissions to the imposed climate varies significantly between the two ecosystem emissions models, the model simulations do not reproduce sufficient emission changes to satisfy ice-core observations of CH$_4$ increases during abrupt events. The inclusion of permafrost physics and peatland carbon cycling in one model (LPJ-WHyMe) increases the climatic sensitivity of CH$_4$ emissions relative to the Sheffield Dynamic Global Vegetation Model (SDGVM) model, which does not incorporate these processes. For equilibrium conditions this additional sensitivity is mostly due to differences in carbon cycle processes, whilst the increased sensitivity to the imposed abrupt warmings is also partly due to the effects of freezing on soil thermodynamics. These results suggest that alternative scenarios of climatic change could be required to explain the abrupt glacial CH$_4$ variations, perhaps with a more dominant role for tropical wetland CH$_4$ sources.

1 Introduction

Dansgaard–Oeschger (D–O) cycles are chiefly characterised by a series of 25 incredibly abrupt warming episodes which occurred during the last glacial period. These events have been reconstructed from Greenland ice-core data (e.g. NGRIP Project Members, 2004; Wolff et al., 2010) and from an increasing number of palaeoclimate proxies from across the globe (e.g. Peterson et al., 2000; Hendy and Kennett, 2000; Wang et al., 2001; Kanner et al., 2012). D–O events typically constitute abrupt warmings of 8 to 16 °C in Greenland which take place over 10–40 yr (e.g. Huber et al., 2006). These temperature transitions were also accompanied by abrupt changes in atmospheric CH$_4$, N$_2$O, dust and δD of ice (e.g. Huber et al., 2006; Wolff et al., 2010), suggesting large-scale abrupt climatic changes which present a challenge to our understanding of natural climatic variability (Seager and Battisti, 2007).

At present D–O climate events are poorly understood, and there remain a number of different hypotheses of their causation (e.g. Clement and Peterson, 2008; Liu et al., 2009; Li et al., 2010; Petersen et al., 2013). The predominant theory

revolves around non-linear changes in the deep-water formation in the North Atlantic Ocean associated with the Atlantic meridional overturning circulation (AMOC) and its northwards heat transport. Abrupt climate transitions in a glacial state have been demonstrated in intermediate complexity climate models (e.g. Ganopolski and Rahmstorf, 2001), but the behaviour in fully coupled general circulation models appears fundamentally different (Liu et al., 2009), relating to changes in the strength of the AMOC rather than the latitudinal position. This is potentially as a result of the inclusion of feedbacks from a dynamic atmospheric model (Yin et al., 2006).

Atmospheric CH$_4$ is one of the few quantities recorded in Greenland ice (Flückiger et al., 2004; Spahni et al., 2005), which suggests widespread climatic anomalies during D–O events, and it potentially provides quantitative constraints on the nature of D–O events. Ice-core data show that CH$_4$ shifts during D–O warming events can be large, ranging up to two thirds of the glacial–interglacial (G–IG) range, i.e. rapid increases of up to 200 ppbv (as the amplitude of the CH$_4$ changes is modulated by orbital parameters) (Huber et al., 2006; Flückiger et al., 2004; Wolff et al., 2010). Ice-core data on the interpolar gradient of CH$_4$ as well as its isotopic signature allow for top-down estimates of the changes in sources during past climate and in general suggest that wetland emissions played a significant role in past atmospheric CH$_4$ variations. Recent improvements in the determination of the interpolar gradient of CH$_4$ from ice-core measurements suggest that low-latitude sources made the dominant contribution to abrupt changes in atmospheric CH$_4$ during the last glacial period (Baumgartner et al., 2012) in agreement with Brook et al. (2000). This result updates older measurements by Dällenbach et al. (2000) which had previously strongly implied that high-latitude sources played an important role during these abrupt events.

Hopcroft et al. (2011) used the Sheffield Dynamic Global Vegetation Model (SDGVM) (Woodward et al., 1995; Beerling and Woodward, 2001) to simulate the global wetland CH$_4$ emission responses in a series of different climate simulations with large AMOC perturbations. Globally the simulated CH$_4$ changes translated into atmospheric increases ranging from 50 to 110 ppbv, and were considered too small to be reconciled with ice-core observations, especially the changes in emissions from the Northern Hemisphere extratropics. By contrast the model has been used to predict the longer orbital-scale changes in atmospheric CH$_4$ of the last 120 kyr successfully (Singarayer et al., 2011). The weak response to abrupt changes was thought to result either from deficiencies in the climate scenario or the sensitivity of the CH$_4$ emission model employed within SDGVM (modified from Cao et al., 1996). For example, SDGVM does not simulate the difference between air and soil temperatures. Hence it does not directly include the influence of freezing on soil moisture availability and does not include vertical discretisation of thermodynamics in the soil which could

be crucial for correctly simulating abrupt changes in CH$_4$ emissions. Additionally, the climate simulations of Hopcroft et al. (2011) were idealised, pertaining either to the LGM (Last Glacial Maximum: 21 kyr BP) or to some idealised boundary conditions (e.g. LGM with altered orbital insolation). This complicated the direct comparison with D–O events which show great variability, especially in terms of the amplitude of abrupt CH$_4$ rises, which are thought to arise through the influence of longer term changes in atmospheric CO$_2$ and orbital insolation values (e.g. Flückiger et al., 2004).

Here we focus on the potential responses of the northern boreal wetlands at specific time periods relevant for understanding the D–O CH$_4$ anomalies. We used the FAMOUS (Smith et al., 2008) coupled atmosphere–ocean general circulation model (GCM) to simulate the global climate of five time periods during the last glacial period driven by estimates of the major climatic forcings: orography, land ice and sea level, trace gases, insolation and freshwater input, the latter leading to strong AMOC (Atlantic meridional overturning circulation) changes. The simulated climates are then used to drive the dynamic vegetation model LPJ-WHyMe (Wania et al., 2009a, b, 2010) and for comparison SDGVM to simulate the response of the northern peatlands and permafrost to abrupt climate changes in the North Atlantic region. LPJ-WHyMe is a development of Lund-Potsdam-Jena (LPJ) (Gerten et al., 2004) and includes representations of permafrost thermodynamics and hydrology and peatland carbon cycling and methane emissions. The comparison with SDGVM allows an assessment of changes to sensitivities that are caused by the presence of these additional processes as compared with a more generalised wetland CH$_4$ scheme. This modelling set-up is used to test assumptions about the climate–CH$_4$ coupling of D–O warming events and to investigate the potential for constraints on mechanisms of climate change during these abrupt transitions.

2　Methods

2.1　Coupled GCM simulations

We performed a series of coupled atmosphere–ocean climate model simulations using the FAMOUS coupled general circulation model (Smith et al., 2008), a low-resolution version of HadCM3 (Gordon et al., 2000). FAMOUS has a horizontal resolution of $7.5° \times 5°$ in the longitude/latitude in the atmosphere and $3.75° \times 2.5°$ in the ocean. The model has 11 and 20 unequally spaced vertical levels in the atmosphere and ocean respectively. The model is configured following the methods of Singarayer and Valdes (2010) for the time periods considered: the LGM, 14, 38, 44 and 60 kyr, where the latter four are close to times of significant D–O events as shown in Table 1. In all simulations the ice sheets, land–sea mask and sea level are altered according to ICE-5G (Peltier, 2004);

Table 1. Comparison of GCM and emission model simulations and ice-core data for Greenland (Blunier and Brook, 2001; Flückiger et al., 2004; Masson-Delmotte et al., 2005; Huber et al., 2006; Wolff et al., 2010).

Time	D–O no.	ΔT wrt PI °C	GCM wrt PI °C	ΔT D–O °C	GCM GI–HS °C	ΔCH_4 D–O ppbv	SDGVM GI–HS ppbv	LPJ-SDGVM GI–HS ppbv
14 kyr	1	−15	−10.7	11	8.8	170	108	−20, −15
LGM	–	−20	−19.6	–	7.3	–	44	−9, 13
38 kyr	8	−18	−16.1	11	8.2	140	87	−11, 6
44 kyr	11	−20	−15.7	15	9.1	112	79	−9, 9
60 kyr	17	−19	−15.2	12	9.4	185	84	−14, 6

ΔT and ΔCH_4 are derived from ice-core reconstructions. The LGM case is included for comparison with the work of Hopcroft et al. (2011). GCM Greenland anomalies are averaged over 60–20° W by 70–80° N. LPJ-SDGVM shows the difference between LPJ-WHyMe and SDGVM over the region $\geq 45°$ N. The range encompasses two scenarios of peat area (standard and with extra peat in Europe and North America).

the CO_2, CH_4 and N_2O mixing ratios are prescribed based on Vostok and European Project for Ice Coring in Antarctica (EPICA) ice-core data (Petit et al., 1999; Spahni et al., 2005); and insolation is modified according to the orbital parameters of Berger and Loutre (1991). The vegetation distribution that is prescribed in FAMOUS is based on the pre-industrial (PI) but accounts for changes in land area and ice-sheet distribution. Note that the vegetation distributions within the dynamic vegetation models used in this study are not prescribed and are allowed to evolve dynamically in response to the simulated climate fields. Each simulation is initialised from pre-industrial initial conditions and integrated without freshwater forcing for at least 500 yr.

The subsequent 500 yr simulation includes a freshwater forcing scenario which is designed to produce large changes in the Atlantic meridional overturning circulation (AMOC), which drives an abrupt and large magnitude of warming over Greenland. This is consistent with previous modelling studies (e.g. Ganopolski and Rahmstorf, 2001; Liu et al., 2009; Merkel et al., 2010), though the exact mechanism of abrupt change in freshwater varies between models and is not addressed here. The freshwater input follows that used by Hopcroft et al. (2011), and is prescribed at a maximum rate of 0.5 Sv (1 Sv = 10^6 m^3 s^{-1}) over the North Atlantic between 50 and 70° N followed by a period of linearly decreasing negative freshwater forcing. This forcing leads to a shutdown to essentially no overturning circulation, followed by a reasonably rapid (100 yr) change to a circulation of approximately twice the control value in each time period. We also begin to explore the sensitivity to the freshwater forcing by including an additional LGM simulation with twice the magnitude (amplitude of 1.0 Sv) of freshwater forcing.

2.2 Peatland methane emission model

The peatland CH_4 emissions are calculated using the dynamic global vegetation model LPJ-WHyMe (Lund-Potsdam-Jena Wetland Hydrology and Methane, Wania

et al., 2010), which includes representations of peatland hydrology and the thermodynamics of permafrost to 10 m (Wania et al., 2009a, b). LPJ-WHyMe includes two plant functional types (PFTs) corresponding to C3 graminoids and *Sphagnum* mosses which are specific to wetlands. The carbon cycle simulated within peatland grid cells is hence wetland-specific, in contrast with many previous wetland models which use upland vegetation distributions as a proxy for the carbon balance in wetland grid cells. CH_4 emissions are dependent on the methanogen-available carbon pool, which is calculated from exudates, above- and below-ground and fast and slow carbon pools, which is then weighted by root density. The temperature dependence of microbial activity is based on an activation energy approach which gives more realistic behaviour at low temperatures compared with a formulation which employs a single Q_{10} value. CH_4 emission by plant mediated transport, ebullition (bubbling) and diffusion are modelled separately.

LPJ-WHyMe requires monthly surface air temperatures, precipitation, cloudiness and wet days as well as the atmospheric CO_2 concentration. In this work the prescribed CO_2 level takes the same value as in the respective FAMOUS GCM simulation, and output from the transient FAMOUS experiments is used for the remaining variables, with the exception of wet days, which is not directly simulated. To overcome this we calculate an exponential regression coefficient between the Climatic Research Unit (CRU) precipitation and wet-day observations (1961–1990) (New et al., 1999) and then used this relationship to calculate a model-derived wet-day field using the model-simulated precipitation. The wet-day field is applied as a climatology calculated from the initial 30 yr mean values from each FAMOUS simulation. This approach assumes that the modern-day relationship between the precipitation and wet-day variables can be used in the other time periods examined in this study.

LPJ-WHyMe requires specification of the area-considered peatland soils. The model then interactively simulates the vegetation distribution, carbon balance, hydrology and CH_4

emissions in each grid cell of peat as a function of input climate. For the pre-industrial, this peat distribution is derived from the International Geosphere–Biosphere Programme soil map of carbon-rich northern soils (Wania et al., 2009a). Pre-Holocene peatland distributions can be inferred from assemblages of peat-core radiocarbon basal dates back to around 16 kyr BP. For example, MacDonald et al. (2006) and Yu et al. (2010) derive time-slice maps of global peatland formation in northern areas and globally. These assemblages can then be extrapolated to give an estimate of the total peatland area through time, assuming linear time dependence of areal expansion around core sites (see Korhola et al., 2009, and Reyes and Cooke, 2011, for some discussion of limitations to this type of approach).

As a first-order approach we took the current peatland areas and mapped these to palaeo-time-periods taking account of land ice (Peltier, 2004) and areas of new land. This gives relatively good agreement with reconstructions (Yu et al., 2010), as this results in almost complete removal of North American and European peat areas at the LGM, although it has less impact on the Siberia peatland distribution. The total peat soil area is reduced by a factor of 32 %, but the reduction is more extreme in North America, where the only remaining peatlands are in Alaska. For the other Marine Isotope Stage (MIS) 3 time periods, the peat area is similar to the LGM as the ice area prescribed (based on ICE-5G) is similar (though its peak height is substantially lower), but as sea level is higher, the total area in some coastal regions of the model is smaller than at the LGM. Recent modelling developments include the dynamic simulation of peatland extent changes from the LGM to Holocene (Spahni et al., 2013), and future work could extend this to the time periods considered in this work.

Sphagnum spores and peat basal dates both indicate southwards expansions of peatlands into the American Midwest and the east coast of the USA during the deglaciation between 16 and 12 kyr (Halsey et al., 2000; MacDonald et al., 2006). In Europe there is less direct pollen- or core-based evidence during the deglaciation, but van Huissteden (2004) presents some evidence for the expansion of peat layers in northern Europe during MIS 3, also a time period of abrupt shifts in atmospheric CH$_4$. As sensitivity tests, we considered two extra scenarios for each palaeo-time-period. The first is the complete removal of the Siberian peat complex in order to match the model peat map to the late glacial distribution of Yu et al. (2010). The second involves introducing new peat grid cells in North America and Europe. Over North America, 0.35×10^6 km^2 (equivalent to 35 % of the modern distribution for North America) of peatland was prescribed in the area south-west and east the Great Lakes consistent with the areal estimate of Halsey et al. (2000) (their Fig. 8), whilst a similar area of peatland was added in northern Europe for comparison. It should be noted that rapid, dynamic changes in peatland area may not be represented in the reconstructions of peat area through time.

The equilibration time for the soil carbon in LPJ-WHyMe is of the order of 1000s of years (Wania et al., 2009b). We tested LPJ-WHyMe under LGM simulations, with a 2000 and a 10 000 yr spin-up length. We then forced the two resultant model states with the transient LGM climate changes including the cooling and abrupt warming. The resultant CH$_4$ emissions time series showed no significant differences. We thus employed a 2000 yr spin-up for each simulation used in this work.

CH$_4$ fluxes simulated by LPJ-WHyMe must be corrected for the overestimate of modern observed peatland area prescribed in the model, as well as for the effect of microtopography which is not explicitly modelled (Spahni et al., 2011). The latter correction takes the value of 0.75, whilst the areal correction factor used here is 0.30 (cf. 0.38 in Spahni et al., 2011), giving a total peatland area in the pre-industrial of 3.20×10^6 km^2

In this work for comparison purposes we also make use of the SDGVM (Sheffield Dynamic Global Vegetation Model Woodward et al., 1995; Beerling and Woodward, 2001), which includes a generalised wetland CH$_4$ model (e.g. Valdes et al., 2005; Singarayer et al., 2011). SDGVM uses upland PFTs to represent the carbon cycling in wetlands, includes nitrogen cycling of both above- and below-ground stores and incorporates eight soil carbon pools. In this generalised scheme, the different pathways of CH$_4$ transport from the soil to the atmosphere are not treated separately. Though emissions are not allowed when the temperatures reach freezing, SDGVM does not currently include the impact of freezing of soil water on plant water availability. The potential wetland area is calculated from the simulated soil moisture in SDGVM, and emissions are calculated on a monthly basis as a function of soil respiration, surface temperature, water table depth and subgrid orography. SDGVM takes account of soil texture and topography. For simulations in which the prescribed sea level is lower than present day, the newly exposed land soil texture is extrapolated from the values of the nearest land points. The subgrid topography is derived from bathymetry data. By contrast LPJ-WHyMe does not take account of variations in soil texture within the peat cells, and so over new land points, the model is only dependent on whether or not peat is prescribed. Similarly, LPJ-WHyMe is not currently dependent on topographic data.

SDGVM emissions are corrected to give the same pre-industrial total of 147 Tg CH$_4$ yr^{-1}, the value used in atmospheric chemistry simulations by Valdes et al. (2005) and Levine et al. (2011). This also means that the pre-industrial northern extratropical flux ($\geq 45°$ N) is very similar in SDGVM and LPJ-WHyMe. SDGVM and LPJ-WHyMe are very different in terms of processes resolved, and show different levels of sensitivity of CH$_4$ emissions to environmental factors (e.g. Wania et al., 2013; Melton et al., 2013). The major differences between the two models are summarised in Table 2.

Table 2. Principal differences between LPJ-WHyMe and SDGVM relevant to the simulation of CH$_4$ emissions.

|	SDGVM	LPJ-WHyMe
Carbon cycle	Upland 6 PFTs	Wetland 2 PFTs
Carbon substrate	Multi-pool H_r^*	Multi-pool H_r^*
Temperature dependence	$Q_{10} = 1.5$	Activation energy
Transport pathways	No	Ebullition, diffusion, plant
Soil thermodynamics	No	Vertically discretised to 10 m
Freeze–thaw	No	Yes
Hydrology	Following Cao et al. (1996)	Following Granberg et al. (1999)
Potential wetland	From soil moisture	Prescribed peat area
Nitrogen cycle	CENTURY model	No

* H_r denotes soil heterotrophic respiration.

3 Results

The palaeoclimate GCM simulations are summarised in Table 1 and compared with temperature anomalies derived from ice-core temperature reconstructions. FAMOUS shows more extreme cooling during the LGM and MIS3 time periods than equivalent simulations with HadCM3 (Singarayer and Valdes, 2010). For example, the cooling over Greenland (which can be compared with ice-core reconstructions) at the LGM relative to the pre-industrial is 20 °C in FAMOUS, compared to around 14 °C in HadCM3.

The changes in AMOC which are the principal drivers of the simulated abrupt change are shown for the three phases of each simulation in Fig. 1. The non-forced phase (with no prescribed freshwater input) of each simulation is denoted EQ, whilst the cold and warm phases are denoted HS (Heinrich stadial) and GI (Greenland interstadial) respectively. These definitions are applied loosely since the climatic forcings which cause the oscillations observed in ice-core data are unknown. The model EQ AMOC values are relatively stable across the different time periods at around 20 Sv (1 Sv $= 10^6$ m^3 s^{-1}), which is consistent with the pre-industrial value of 18 Sv, and this is close to the observational estimates of modern overturning strength in the Atlantic of 18 Sv $\pm$ 3–5 (Talley et al., 2003). The large changes in AMOC forced by freshwater input are also similar amongst the different simulations, especially when considering the considerable interannual variability as shown by the vertical bars. The only exception is the $\pm$1.0 Sv LGM simulation for which the HS AMOC value is weaker than the corresponding HS phases in the remaining simulations. In the 0.5 Sv simulations, the AMOC varies between an average HS value of around 5 Sv and a GI value of 35 Sv.

The pattern of GI–HS warming is shown in Fig. 2 for the mean for four of the simulations. The patterns in the remaining time periods are similar to those of the 38 kyr model and are not shown. In all cases there is a clear contrast between the land and ocean response, with a larger signal over ocean. Over Eurasia the annual mean warming is generally stronger
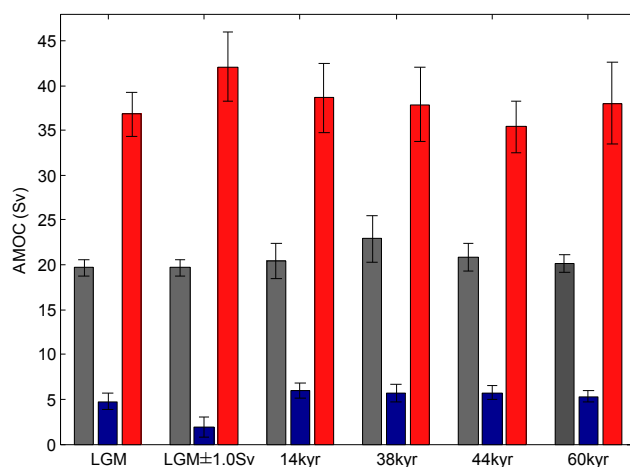
Fig. 1. 30 yr mean $\pm$1 standard deviation Atlantic meridional overturning circulation (AMOC) values for the three phases of each climate simulation: grey for EQ (equilibrium), blue for HS (Heinrich stadial-like) and red for GI (Greenland interstadial-like).

than over North America, although this difference is minimal in the summer mean. The differences between the 0.5 Sv simulations (LGM, 14 and 38 kyr) are relatively small, indicating a reasonably low sensitivity to the different boundary conditions imposed, such as the lower ice sheets or atmospheric CO$_2$. FAMOUS shows more sensitivity to the magnitude of freshwater forcing, as the $\pm$1.0 Sv LGM simulation shows amplified temperature changes, particularly over the North Atlantic and Europe.

The abrupt changes over Greenland are also compared with reconstructions derived from ice cores in Table 1. In the model (averaged over 60–20° W, 70–80° N) the total warming (GI–HS) ranges from 7.3 to 9.4 °C, which is at the lower end of the estimates of Greenland warming (see column 3, Table 1). The model temperature anomaly averaged over a box located further southwards displays a larger magnitude. For example over the range 60–80° N by 60–20° W, the maximum warming is 11.1 °C. This implies that, were the model
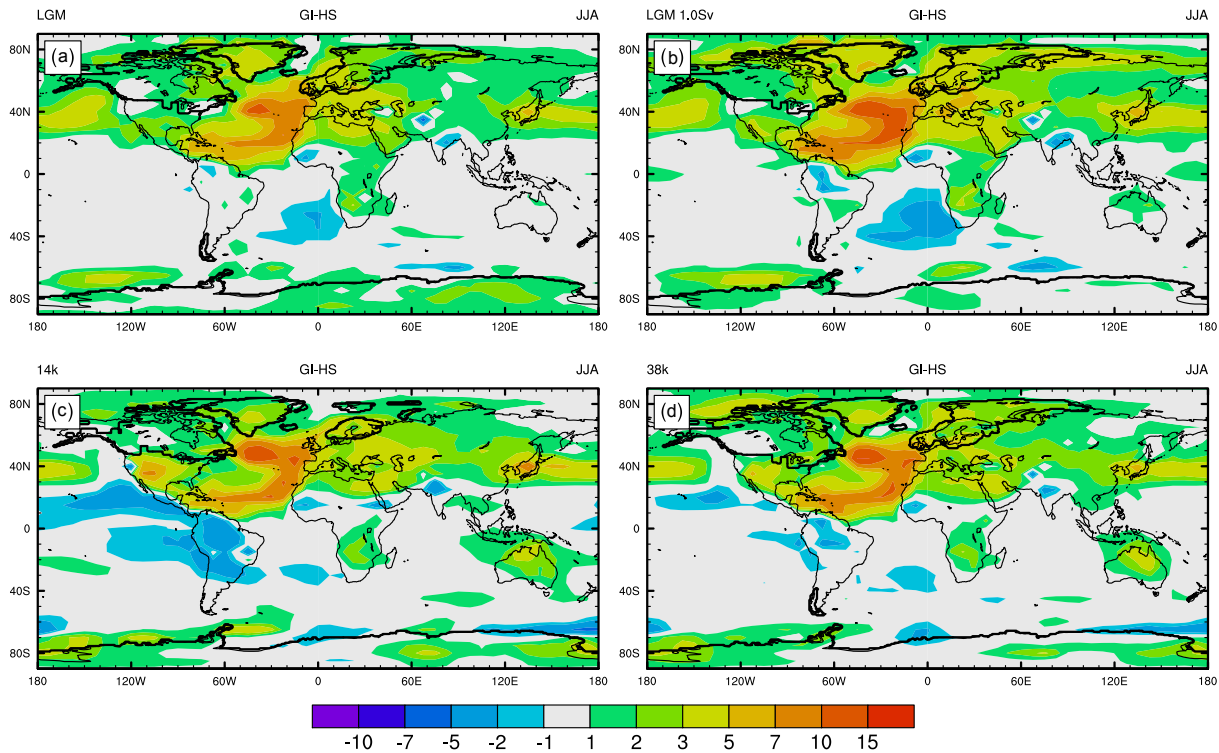
Fig. 2. Summer (JJA) GI–HS surface temperature anomalies (°C) in simulations with boundary conditions relevant to **(a)** the LGM, **(b)** the LGM with double the freshwater forcing compared with the other simulations, **(c)** 14 kyr and **(d)** 38 kyr. The distribution of land ice in each simulation is shown by the black contour line.

to simulate a more northwards penetration of the oceanic heat transport, the temperature signal over Greenland may be in better agreement with the changes inferred from Greenland ice cores, but other processes missing in this idealistic freshwater forcing scenario could also be important.

Equivalent precipitation anomalies are shown in Fig. 3, where the asymmetric response between North America and Eurasia is also seen. Generally the signal is again stronger over the ocean. The precipitation changes in all seasons are minimal over North America, and for coastal grid cells show a drying, which is opposite of the small increases in precipitation simulated over much of western Eurasia.

3.1 Comparison of climate anomalies with reconstructions

A variety of proxy data record abrupt glacial climate change from across the Northern Hemisphere and could serve as indicators of potential mechanisms. Speleothems from China (Wang et al., 2001) show strong correlation with millennial variability of Greenland ice cores, suggesting more intense summer monsoons in China during Greenland interstadial phases. Global pollen records of sufficient temporal resolution are relatively sparse but have been collated globally for important D–O events (Harrison and Sanchez-Goñi, 2010). For the transition during D–O 8, these records

indicate significant increases in temperature in Europe and eastern North America, whilst significant changes to plant available moisture occur mainly in Europe, with a more complex pattern of both increases and decreases over tropical South America. Changes in the intertropical convergence zone (ITCZ) precipitation are also inferred for the Cariaco Basin which is located at 10° N on the coast of Central America (Peterson et al., 2000).

The abrupt transitions in these simulations lead to large changes in annual and especially winter temperatures and precipitation over Europe and the North Atlantic. There is also a concurrent southwards shift in the ITCZ during the HS phase similar to previous modelling studies. There is no northwards shift of the ITCZ in the GI relative to the EQ phase (Hopcroft et al., 2011). There is no significant change in the Asian monsoon in contrast to the speleothem reconstructions, but there is a strong decrease in the strength of the summer Indian monsoon system during the cool HS phase. This is similar to the results of Pausata et al. (2011). There is no significant change in the Indian or Asian monsoons in the warm GI phase relative to the unperturbed EQ phase. The precipitation anomaly pattern over South America is complex and shows increases over the northern part of the continent with a strong decrease over the Atlantic coastal areas. This is broadly consistent with opposing signals inferred from speleothem at locations 10° S and 11° N (Kanner et al.,
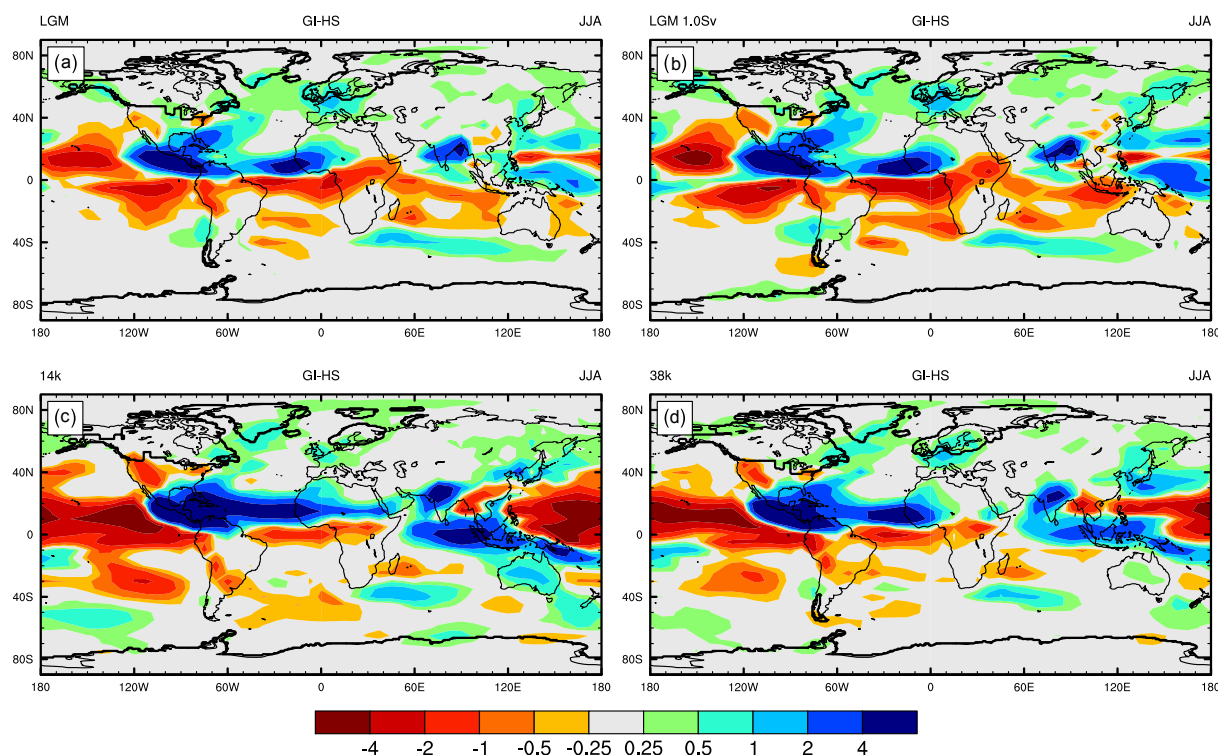
Fig. 3. As in Fig. 2 but showing summer (JJA) GI–HS precipitation anomalies (mm day^{-1}). The distribution of land ice in each simulation is shown by the black contour line.

2012; Peterson et al., 2000, respectively), but the pattern of changes is not in particularly good agreement with inferences from pollen data (Harrison and Sanchez-Goñi, 2010) for D–O event 8.

Gherardi et al. (2005) inferred approximately a 10 °C increase in sea surface temperature (SST) during the Bølling–Allerød at a site in the western Atlantic at 37° N. This is comparable with the modelled annual mean GI–HS warming in the 14 kyr simulation in this region. Elliot et al. (2002) reconstructed 7 and 3.5 °C summer SST warmings at a site in the western Atlantic at 55° N for the Bølling–Allerød and D–O 8, respectively. The former is consistent with the model simulations, although the annual mean warming at this location is much larger in the model, but the latter is much smaller than simulated for the 38 kyr event. Further north at site SO82-5 (59° N), van Kreveld et al. (2000) inferred oscillations of 4 °C, which is around a factor of 4 smaller than the changes simulated in the model in any time period. Other SST estimates of both winter and summer change for D–O 8 are summarised by Harrison and Sanchez-Goñi (2010) and show SST increases of 8–10 °C in both seasons for sites at latitude 37–45° N in the Atlantic. These changes are consistent with the modelled change in summer, but the winter temperature change is larger in the model, which is in places larger than 15 °C. The model fails to reproduce the 3–5 °C warming over the Santa Barbara Basin inferred by Hendy and Kennett (2000). The majority of these changes appear to be replicated

to some extent in the model simulations. Notable exceptions are the absence of adequate warming in the Santa Barbara Basin in the model and the potential overestimation of SST changes in the high-latitude North Atlantic.

3.2 CH₄ emissions in each time period

The prescribed extratropical peatland area for the LGM is $2.2 \times 10^6 \ km^2$, with similar values for the remaining time periods as summarised in Table 3. The base EQ emissions in LPJ-WHyMe in the time periods considered vary from $33.6 \ Tg \ CH_4 \ yr^{-1}$ in the pre-industrial to only $1.9 \ Tg \ CH_4 \ yr^{-1}$ at the LGM as shown in Fig. 5 and summarised in Table 3. For comparison when forced with CRU 1961–1990 climatology regridded to FAMOUS resolution and a CO_2 value of 280 ppmv, the boreal (> 45° N) peatland source is $31.0 \ Tg \ CH_4 \ yr^{-1}$. Both of these values are similar to the range of 38.5–$51.1 \ Tg \ CH_4 \ yr^{-1}$ simulated by Spahni et al. (2011), and are within the range of inverse estimates of $33 \pm 18 \ Tg \ CH_4 \ yr^{-1}$ (Chen and Prinn, 2006).

The LGM value reduces to $0.9 \ Tg \ CH_4 \ yr^{-1}$ when the Siberian peatlands are removed. The baseline rates at 38 and 14 kyr are intermediate at 4.9 and $11.1 \ Tg \ CH_4 \ yr^{-1}$ respectively, and these reduce to 1.2 and $4.0 \ Tg \ CH_4 \ yr^{-1}$ without the sources located in Siberia. The warmer climate and higher CO_2 level at 14 kyr stimulate the Asian peatlands so that emissions are higher than during the 38 kyr

Table 3. CH$_4$ emissions in LPJ-WHyMe and as inferred from observations. *no Sib* indicates that the Siberia peat complex is omitted, and *NA + EU* denotes extra peatland areas introduced in North America and Europe as described in the main text. All forcing climates are as simulated directly by FAMOUS, except LPJ-WHyMe (CRU) which is forced with regridded 1961–1990 mean climatological observations (New et al., 1999). ± 1.0 Sv denotes the transient LGM simulation with double the magnitude of freshwater forcing.

Time	Model/obs	Experiment	[CO$_2$]	Area	CH$_4$ emissions			
			ppmv	10^6 km^2	Tg CH$_4$ yr^{-1}			
				EQ	EQ	HS	GI	GI–HS
PI	obs/inversion			2.99–4.0[a]	33 ± 18[b]	–	–	–
	LPJ-WHyMe (CRU)		280	3.2	31.0	–	–	–
	LPJ-WHyMe	PI control	280	3.2	33.6	–	–	–
14 kyr	LPJ-WHyMe	14 kyr control	237	2.2	11.1	7.6	15.1	7.5
		no Sib		0.25	4.0	1.8	6.1	4.3
		no Sib + NA + EU		0.42	14.0	12.1	18.4	6.2
		+ NA + EU		2.37	21.1	17.9	26.3	8.4
LGM	LPJ-WHyMe	LGM control	185	2.2	1.9	0.6	3.5	2.8
		LGM + PI CO$_2$	280	2.2	4.0	2.0	6.2	4.2
		no Sib	185	0.32	0.9	0.1	1.6	1.5
		no Sib + NA + EU		1.1	6.2	3.9	11.9	8.0
		+ NA + EU		3.0	7.3	4.4	13.5	9.1
LGM	LPJ-WHyMe	± 1.0 Sv	185	2.2	1.9	0.4	4.0	3.6
38 kyr	LPJ-WHyMe	38 kyr control	211	2.1	4.9	2.2	5.9	3.7
		no Sib		0.15	1.2	0.4	2.1	1.7
		no Sib + NA + EU		0.31	10.8	7.8	14.6	6.8
		+ NA + EU		2.26	14.4	9.7	19.1	9.4
44 kyr	LPJ-WHyMe	44 kyr control	213	2.3	4.6	3.0	6.1	3.1
		no Sib		0.3	1.0	0.7	2.0	1.2
		no Sib + NA + EU		1.1	10.1	8.3	15.0	6.7
		NA + EU		3.1	13.6	10.6	18.9	8.2
60 kyr	LPJ-WHyMe	60 kyr control	211	2.3	4.2	2.5	5.8	3.3
		no Sib		0.3	1.2	0.7	2.2	1.5
		no Sib + NA + EU		1.1	10.1	8.1	14.6	6.5
		+ NA + EU		3.1	13.1	10.0	17.6	7.7

[a] Spahni et al. (2011); Yu et al. (2010); [b] Chen and Prinn (2006).

climate, despite similar orbital insolation patterns at northern latitudes. The mean emissions are 11.1 compared to only 4.9 Tg CH$_4$ yr^{-1} in the 38 kyr simulation. The inferred northern (three-box model) LGM source of Baumgartner et al. (2012) is around half the late Holocene value. Whilst the LPJ-WHyMe results show a very strong reduction in the peatland emissions, this peatland source is not directly comparable with the northern source inferred from the interpolar CH$_4$ gradient which additionally includes subtropical regions.

3.3   Transient CH$_4$ emissions in LPJ-WHyMe

The peatland emissions respond relatively strongly to the transient changes in climate induced by the freshwater perturbation. The transient decadally averaged CH$_4$ emissions

in LPJ-WHyMe are shown together in Fig. 6. The marked response is especially evident in the 14 kyr simulation, where although the fractional increase in emissions is only 36 % during the warm (GI) phase relative to the unforced (EQ) initial stage, the absolute change is 4 Tg, larger than the increases during the other time periods, which are 1.6 and 1.0 Tg yr^{-1} in the LGM and 38 kyr simulations respectively. The magnitude of the transition from GI to HS (i.e. the largest change in each simulation) ranges from 2.8 to 7.5 Tg CH$_4$ yr^{-1} in the LGM and 14 kyr simulations respectively. For comparison we also plot the transient changes in the water table depth and thaw depth in Fig. 7. This shows that water table depths are probably less important than changes in the thaw depth for determining the CH$_4$ emissions changes, a point we return to in more detail in the model
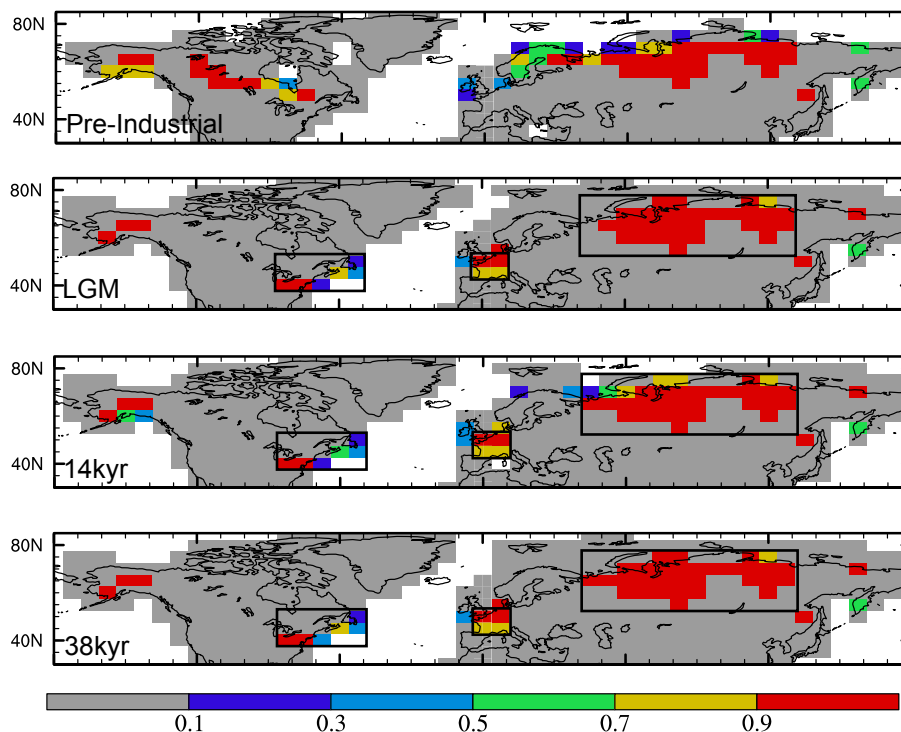
Fig. 4. Prescribed peat grid cells in the pre-industrial, LGM, 14 and 38 kyr simulations. Boxes indicate area of peat removed (for Siberia) or additionally prescribed (for western North America and Europe) as summarised in Table 3.
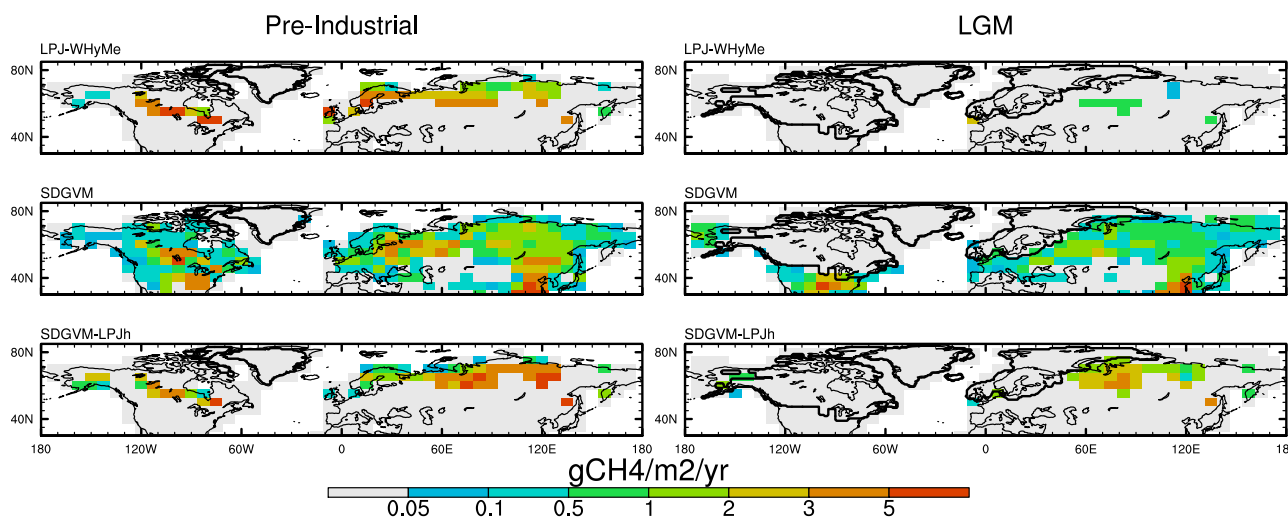

Fig. 5. CH$_4$ emissions for PI and LGM conditions for LPJ-WHyMe, SDGVM and SDGVM-LPJ-h, including a correction for the fractional land area in coastal grid cells. The distribution of land ice in each simulation is shown by the black contour line.

comparison section. We also see the dominant influence of the abrupt warming on thaw depth, but this is not the case for the water table depth, which appears to respond on a slower response time, with the very slight deepening of the water table depth during the abrupt cooling persisting until after the abrupt warming has occurred.

The spatial pattern of GI–HS emission anomalies is shown for these two simulations in Figs. 8 and 9. The largest anomalies are seen over Europe. The GI–HS change in the 14 kyr simulation shows a similar feature but a larger area of significant emissions anomalies.

Removing the peat area in Siberia (as shown in Fig. 4) reduces the EQ emission rates by more than 50 % in each
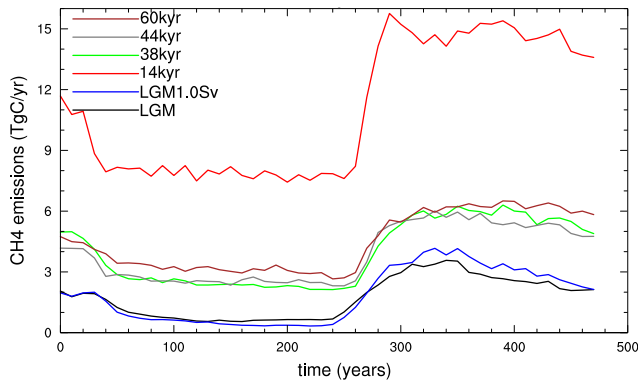
Fig. 6. Decadally averaged mean CH_4 emission time series in LPJ-WHyMe for the five different palaeoclimate simulations.

Fig. 7. Decadally averaged (northwards of 45° N) water table depth and thaw depth in the LPJ-WHyMe simulations. The pre-industrial simulated mean ±2 standard deviations (dashed lines) are shown for comparison.

time period. Consequently the abrupt response (GI–HS) is also reduced, but by less than 50 %. Prescribing extra areas of peat near the North Atlantic in Europe and North America results in a significant increase in emissions. In the 14 kyr simulation, the EQ emission increases from 11.1 to 21.1 Tg CH_4 yr^{-1} and in the 38 kyr simulation from 4.9 to 14.4 Tg CH_4 yr^{-1}. Similarly the GI–HS response is larger, giving abrupt changes that range from 7.7 to 9.4 Tg CH_4 yr^{-1} in the 60 and 38 kyr simulations respectively.

4 Analysis

4.1 Comparison with the ice-core inferences

The recent interpolar gradient data from Baumgartner et al. (2012) (from NGRIP and EDML) and prior work of Brook et al. (2000) based on GISP2 and Taylor Dome ice cores, both suggest modest emission increases at high latitudes during D–O events, with a more important contribution from subtropical and northern tropical regions. Comparing the LPJ-WHyMe changes in CH_4 emissions across all of the simulations summarised in Table 3, it is clear that the simulated changes will not explain a significant component of the observed D–O event abrupt changes in CH_4. This is consistent with a dominant contribution of tropical sources to abrupt CH_4 changes as inferred by Baumgartner et al. (2012). Furthermore, the relatively minor changes in emissions between the different LPJ-WHyMe simulations are at least partially consistent with the relatively stable contribution from the northern sources through the latter part of the last glacial period as inferred by Baumgartner et al. (2012).

The largest signal occurs in the 38 kyr simulation when the extra NA + EU peat areas are prescribed. The change for the equivalent LGM simulation is 8.4 Tg, and is similarly large because although the temperatures are lower, some of the land areas submerged at 38 kyr are fully exposed at the LGM, increasing the areas of peatland in Europe and eastern North America.
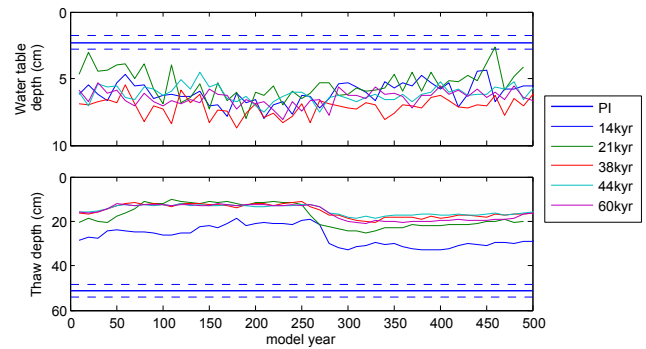
If peatlands can indeed expand rapidly (as suggested by MacDonald et al., 2006), then changes in the emitting area may be an important consideration for the CH_4 budget during D–O events. Furthermore, changes in the latitudinal distribution of wetlands on longer timescales and transitions from fens to bogs (the latter being less productive in CH_4 emissions), which are not considered separately in current models, could be important.

4.2 Comparison with SDGVM

Comparisons are now made between the results from the peatland model LPJ-WHyMe and a wetland model in SDGVM. Since the two models contain largely different representations of soil physics and plant functional types, this comparison should give information on processes important for abrupt CH_4 change and provide some insight into the uncertainty associated with the simulated CH_4 fluxes. The summary values for all of the simulations are shown for comparison with LPJ-WHyMe in Table 4, which shows that SDGVM predicts a much larger area of emissions than any of the prescribed areas used in LPJ-WHyMe. The LGM emissions in SDGVM are also larger than in LPJ-WHyMe. The reductions of emissions at the LGM are 94 and 65 % in LPJ-WHyMe and SDGVM respectively, showing that LPJ-WHyMe is much more sensitive to the LGM low CO_2 and climate conditions. The influence of the lowered atmospheric CO_2 versus the LGM climate can be assessed by running both models forced with LGM climatology but pre-industrial CO_2 levels. Doing so demonstrates that 88 % of the LGM reduction in emissions for these models is due to climate, with only the 12 % as a result of the prescribed reduction in atmospheric CO_2 concentration.

The GI–HS transition for the LGM is 5.3 Tg CH_4 yr^{-1} in SDGVM, and the spatial pattern of GI–HS is shown in comparison with LPJ-WHyMe in Fig. 8. In SDGVM for the boreal region, the wetland area decreases during the cooling (HS) and increases during the warming (GI), but the
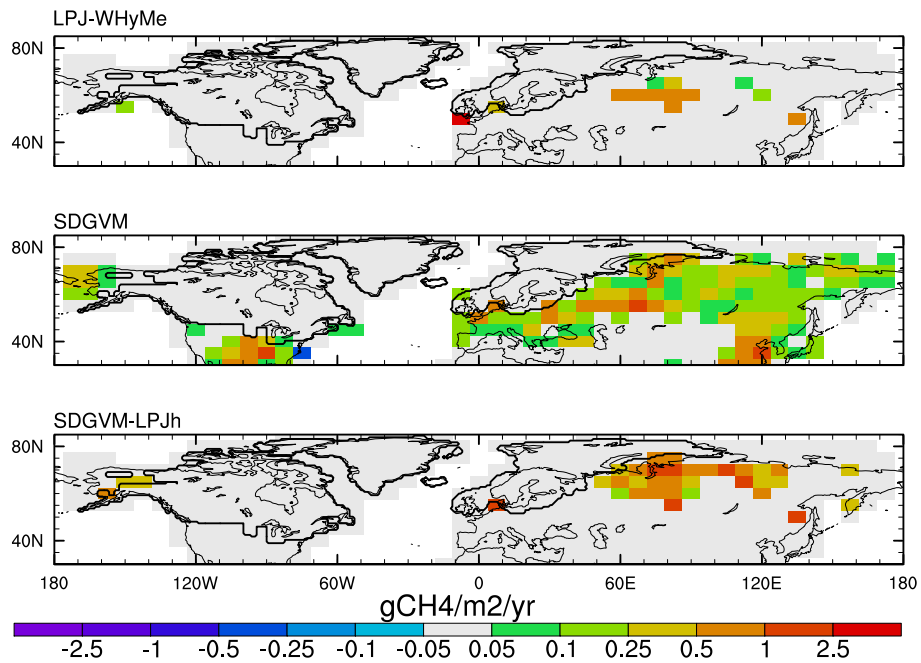
Fig. 8. CH$_4$ emission anomalies for GI–HS for LGM conditions in LPJ-WHyMe, SDGVM and SDGVM-LPJ-h, including a correction for the fractional land area in coastal grid cells. The distribution of land ice in each simulation is shown by the black contour line.
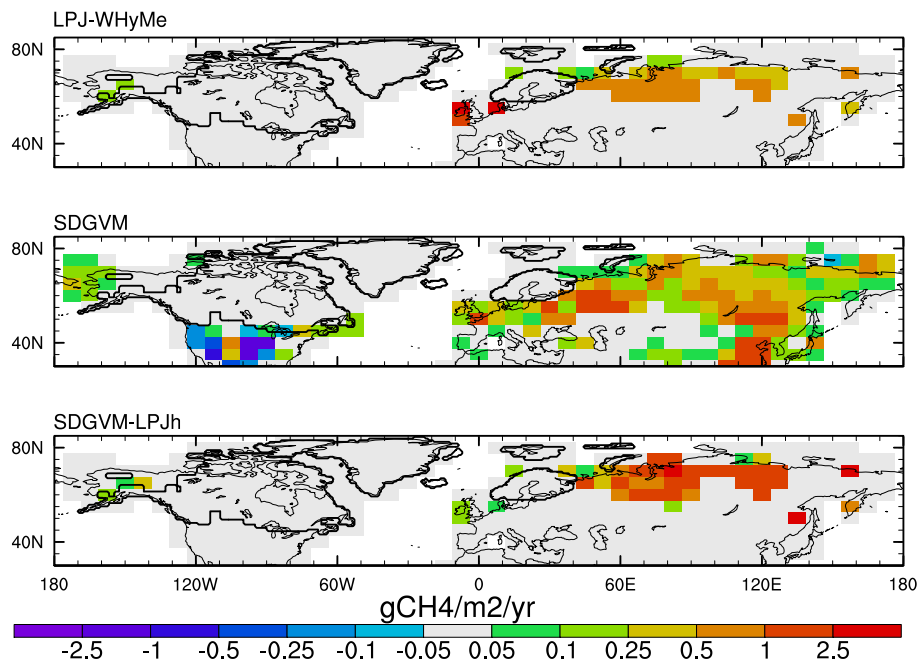
Fig. 9. CH$_4$ emission anomalies for GI–HS for 14 kyr conditions in LPJ-WHyMe, SDGVM and SDGVM-LPJ-h, including a correction for the fractional land area in coastal grid cells. The distribution of land ice in each simulation is shown by the black contour line.

fractional changes are small, and the majority of the change in emissions is a consequence of climatic influence on emission rates rather than changes in the simulated wetland area.

LPJ-WHyMe appears to be more sensitive to the imposed climate, since the proportional changes are larger.

For example, in the LGM simulations the GI–HS change is 153 % of the control LGM value, compared to only 40 % in SDGVM. This may be because the spatial distribution of wetlands is different or due to other internal processes in the model. We explored this aspect more robustly by configuring

Table 4. CH$_4$ emissions in sensitivity simulations with modified model versions and $\geq 45°$ N in SDGVM (this study and Hopcroft et al., 2011). h, R_h and T signify hydrology, soil heterotrophic respiration and soil temperature respectively. These fields are read into the modified versions of SDGVM from LPJ-WHyMe. Wetland area in SDGVM is calculated from the area with the water table depth ≥ 0 cm, but in other models is the area of prescribed peatland.

Time	Model	[CO$_2$]	Area	CH$_4$ emissions			
		ppmv	10^6 km^2	Tg CH$_4$ yr^{-1}			
			EQ	EQ	HS	GI	GI–HS/EQ
PI	LPJ-WHyMe	280	3.2	33.6	–	–	–
	SDGVM		18.3	32.7	–	–	–
14 kyr	LPJ-WHyMe	237	2.2	11.1	7.6	15.1	68 %
	SDGVM-LPJ-hR_hT		2.2	9.6	4.9	13.6	90 %
	SDGVM-LPJ-hR_h		2.2	16.7	14.8	19.7	34 %
	SDGVM-LPJ-h		2.2	33.0	28.7	37.1	26 %
	SDGVM		16.5	33.9	25.5	37.4	35 %
LGM	LPJ-WHyMe	185	2.2	1.9	0.6	3.5	153 %
	SDGVM-LPJ-hR_hT		2.2	2.1	0.1	3.5	158 %
	SDGVM-LPJ-hR_h		2.2	3.6	2.0	4.8	79 %
	SDGVM-LPJ-h		2.2	13.2	9.8	14.5	36 %
	SDGVM		15.0	13.3	10.7	16.0	40 %
LGM $\pm$ 1.0 Sv	LPJ-WHyMe	185	2.2	1.9	0.4	4.0	190 %
	SDGVM-LPJ-hR_hT		2.2	2.2	0.03	4.0	186 %
	SDGVM-LPJ-hR_h		2.2	3.5	1.4	5.3	112 %
	SDGVM-LPJ-h		2.2	13.2	8.6	14.9	48 %
	SDGVM		15.0	13.4	10.1	16.8	50 %
38 kyr	LPJ-WHyMe	211	2.1	4.9	2.2	5.8	74 %
	SDGVM-LPJ-hR_hT		2.1	3.0	0.7	3.9	111 %
	SDGVM-LPJ-hR_h		2.1	9.1	5.1	8.6	39 %
	SDGVM-LPJ-h		2.1	22.3	17.4	24.4	31 %
	SDGVM		14.3	20.2	16.3	23.2	30 %
44 kyr	LPJ-WHyMe	213	2.3	4.6	3.0	6.1	68 %
	SDGVM-LPJ-hR_hT		2.3	2.7	1.5	4.0	95 %
	SDGVM-LPJ-hR_h		2.3	8.4	5.4	9.7	36 %
	SDGVM-LPJ-h		2.3	21.4	17.2	22.3	24 %
	SDGVM		14.3	18.8	15.3	21.0	30 %
60 kyr	LPJ-WHyMe	211	2.3	4.2	2.5	5.8	79 %
	SDGVM-LPJ-hR_hT		2.3	2.7	1.5	5.4	149 %
	SDGVM-LPJ-hR_h		2.3	8.4	5.4	9.7	51 %
	SDGVM-LPJ-h		2.3	25.4	20.4	27.2	27 %
	SDGVM		14.4	21.6	17.7	25.0	34 %

a modified version of SDGVM, here denoted SDGVM-LPJ-h, only for peatland grid cells prescribed in LPJ-WHyMe (in the default configuration). Three other modifications were introduced to SDGVM-LPJ-h in order to minimise differences between the two models: (i) the water-table depth values calculated by LPJ-WHyMe were used instead of those calculated using the SDGVM soil moisture content; (ii) the Q_{10} of CH$_4$ production sensitivity to temperature was increased from 1.5 to 2.0; and (iii) the orographic correction applied in SDGVM to modify the wetland area and flux was removed.

The output of this model then has the same spatial distribution of CH$_4$-producing areas as the equivalent LPJ-WHyMe simulation. The water-table position will implicitly include the effect of soil freezing (from LPJ-WHyMe), whilst the carbon substrate available for methanogenesis (which is still calculated within SDGVM) does not. The total pre-industrial emissions of SDGVM-LPJ-h are scaled to match those of LPJ-WHyMe so that differences between the models are more easily quantified.

The emissions in each simulation are compared in Table 4. The LGM drop in SDGVM-LPJ-h is only 60 % compared with 95 % in LPJ-WHyMe showing that the latter remains more sensitive to the imposed climate anomalies. Further the GI–HS fluctuation in LPJ-WHyMe is still relatively larger than in SDGVM-LPJ-h at 147 % compared with only 36 % in SDGVM-LPJ-h, which is actually lower than the value in SDGVM alone (40 %). This is the result of the different areal extension of CH$_4$-producing areas used in the original and hybrid SDGVM versions, specifically the contributions of the larger area of circum-Atlantic CH$_4$-producing areas (where the climate anomalies are larger) in the original model version.

In order to understand these differences further, the net primary productivities (NPPs) averaged over the prescribed peatland grid points were compared. Whilst both models show a similar PI value of around 2.5 GtC yr^{-1}, SDGVM shows a much smaller change in NPP at the LGM, with a reduction of around 50 % compared to 90 % in LPJ-WHyMe. This could be a result of the inclusion of the nitrogen cycle in SDGVM. Nitrogen uptake by plants is dependent on soil nitrogen, temperature and soil carbon in SDGVM (Woodward et al., 1995). There are also potential differences in the sensitivities of the plant functional types in the two models. This low sensitivity in SDGVM is not evident in transient anomaly time series for the abrupt climate events, for which the absolute changes in NPP in the two models are very similar at around ±0.2 GtC yr^{-1} for the HS and GI phases. The relatively large reduction in NPP simulated by LPJ-WHyMe is much greater especially in the colder climates such as the LGM and 38 kyr than in SDGVM. This is because the initial EQ values are lower than in the corresponding SDGVM simulation. Using NPP to predict CH$_4$ emissions in the different time periods as a linear function of the ratio of NPP (Whiting and Chanton, 1993) in that time period relative to the pre-industrial, we find that this overpredicts emissions in LPJ-WHyMe by up to 89 %, but the maximum error is only ±15 % for SDGVM. This implies that the climate sensitivity of LPJ-WHyMe additionally derives from the processes involved in emissions and transport of CH$_4$ that are not represented in SDGVM. We return to this point in the subsequent analysis.

Taking the same approach for the abrupt transition from HS to GI is less informative as the different carbon stocks, respiration rates and NPP are unlikely to be in equilibrium during the abrupt climate changes. Instead, a further model hybrid is tested in which the SDGVM-LPJ-h now reads the monthly heterotrophic soil respiration H_r from LPJ-WHyMe. This version is called SDGVM-LPJ-hR$_h$. SDGVM-LPJ-hR$_h$ includes both the soil moisture and water table depth and the carbon substrate from LPJ-WHyMe , but still lacks a representation of the processes related to CH$_4$ transport and oxidation through the soil column, or any direct influence due to the position of the active layer depth.

Again emissions are compared for this model version with the previous three models in Table 4. This model shows emissions much closer to those of LPJ-WHyMe. In particular the reduction in emissions at the LGM relative to the pre-industrial is now 89 %, which compares favourably with 94 % in LPJ-WHyMe, and is much larger than the value of only 61 % in SDGVM-LPJ-h. This also supports the scaling of NPP to calculate the EQ emission rates in different time periods. However, this model version (SDGVM-LPJ-hR$_h$) still considerably underestimates the transient emission changes seen in LPJ-WHyMe. For example in the LGM simulation the increase during the GI relative to the EQ is 84 % in LPJ-WHyMe, but only 33 % in SDGVM-LPJ-hR$_h$, though this is far larger than the 10 % in SDGVM-LPJ-h. The values for the warmest simulation (14 kyr) follow a similar pattern: 36 % for LPJ-WHyMe versus 18 % in SDGVM-LPJ-hR$_h$ and 12 % in SDGVM-LPJ-h. Thus whilst the long-term equilibrium (EQ) values can be reconciled by taking the carbon substrate from LPJ-WHyMe in this hybrid model set-up, the transient sensitivity of LPJ-WHyMe cannot.

A final model version SDGVM-LPJ-hR$_h$T now takes the 25 cm soil temperature predicted by LPJ-WHyMe in the SDGVM-LPJ-hR$_h$ model rather than using the surface air temperature simulated by FAMOUS. The 25 cm soil temperature is chosen because it controls the rates of heterotrophic respiration within LPJ-WHyMe for CH$_4$ emissions (Wania et al., 2010). The LGM reduction in emissions in SDGVM-LPJ-hR$_h$T is 94 %, comparable to 95 % in LPJ-WHyMe, and the transient sensitivity is approximately the same in SDGVM-LPJ-hR$_h$T and LPJ-WHyMe (as shown in Table 4). This suggests that the effects of soil freezing and the position of the active layer depth increase the sensitivity of the CH$_4$ emissions in cold regions and that only by including this can we reconcile the magnitude of change in CH$_4$ emissions seen in LPJ-WHyMe with the hybrid model considered here. Other differences remain, particularly in the remaining time periods, and these must be related to other differences between LPJ-WHyMe and SDGVM not considered in the above analysis.

4.3 Concentration predictions

The modelled changes in emissions between the cold and warm states (HS and GI) are now used to calculate the likely change in atmospheric CH$_4$. This allows direct comparison with the ice-core record for all events simulated without the complications arising from deconvolving the emission estimates from the interpolar gradient. Numerical simulations of the major influences on the atmospheric CH$_4$ lifetime during a glacial abrupt warming event suggest that the lifetime may be relatively constant (Levine et al., 2012). Thus we employed a constant lifetime of 8.6 yr (following prior work: Hopcroft et al., 2011) and assumed a uniform conversion of emissions to atmospheric concentration of 2.75 ppbv Tg^{-1}. The results are increased by 10 % to

account for the self-feedback of CH$_4$ on its own lifetime, based on analysis of glacial atmospheric chemistry simulations (Levine et al., 2011). The SDGVM total pre-industrial emissions are scaled to match the value of 147 Tg CH$_4$ yr^{-1} used by Valdes et al. (2005) and Levine et al. (2011) in order to be more consistent with previous calculations of atmospheric concentration changes for glacial time periods. This means that the total concentration predictions are slightly smaller than those predicted in previous work (Hopcroft et al., 2011). The LPJ-WHyMe values are given as differences with the emissions from SDGVM over the equivalent area, to illustrate the effect of the inclusion of more complex model dynamics. Two LPJ-WHyMe scenarios are considered: the standard case and that with extra peatland prescribed in North America and Europe. To avoid double counting in the latter case, the SDGVM emissions are only summed over grid cells below 45° N, which do not contain prescribed peatlands in the equivalent LPJ-WHyMe scenario. The extra areas of peatland are only prescribed in LPJ-WHyMe since the wetland area in SDGVM is calculated dynamically.

The maximum calculated change in atmospheric CH$_4$ calculated by summing SDGVM ($< 45°$ N) and LPJ-WHyMe ($\geq 45°$ N) is 93 ppbv in the 14 kyr case, whilst the maximum total change is only 88 and 90 ppbv in the 44 and 60 kyr cases respectively. Depending on the area of peat prescribed, the LPJ-WHyMe model can simulate both less and more change than in SDGVM, with the exception of the 14 kyr case. The predicted CH$_4$ changes are compared against ice-core data in Table 1. The SDGVM results underestimate the events by 30–55 %. Inclusion of LPJ-WHyMe only improves the agreement with ice-core data when the maximum peat area simulations are used in the LGM, 38, 44 and 60 kyr simulations. In these simulations LPJ-WHyMe increases the change by up to 10 %. Despite the increased transient sensitivity of the LPJ-WHyMe model, the results still suggest underestimation of the observed rapid CH$_4$ increases. This is partly because LPJ-WHyMe predicts lower initial (EQ) emissions than SDGVM during each time period.

The significant variation in the amplitude of the abrupt CH$_4$ changes as evident from the ice-core data (Flückiger et al., 2004; Huber et al., 2006) does not appear to be well replicated in the simulations. For example, the CH$_4$ change at D–O event 17 is 65 % larger than for event 11. Singarayer et al. (2011) demonstrated that the SDGVM model is able to replicate the orbital timescale changes in CH$_4$ emissions rather well. Hence the lack of variability in the size of the abrupt changes simulated here could result from some feature of the physical climatic forcing. The abrupt changes simulated in response to variations in the AMOC are very similar in the different time periods considered as shown in Figs. 2 and 3. Whilst the changes in AMOC are the key mechanism of climatic change explored in this work, they are not involved to such a strong degree in the simulations of Singarayer et al. (2011). This difference could help to explain why the model simulations here cannot explain the full magnitude of change, whereas the SDGVM model results of Singarayer et al. (2011) can successfully explain the longer term glacial–interglacial modulations. Deficiencies in the scenario employed (i.e. the freshwater forcing) or in the GCM response to this freshwater forcing (e.g. because oceanic eddies are not resolved) could be important considerations in this regard.

5 Discussion

We have performed a series of transient coupled GCM simulations of five time periods considered important for Dansgaard–Oeschger events of the last glacial period. Using freshwater forcing to perturb the model AMOC, we instigate rapid warming in the North Atlantic region, mostly as a result of increased heat transport from the resurgent AMOC, but also partly deriving from feedbacks from sea-ice cover and atmospheric heat transport. The warming over Greenland in the model is of the order of 8–9 °C, which is at the lower end of the ice-core reconstructions. Doubling the magnitude of the freshwater forcing (which equates to 10 m/century sea-level rise) does not reproduce the largest magnitude of warming observed in Greenland of up to 16 °C (Huber et al., 2006; Wolff et al., 2010).

The inferred source changes for northern sources from recent data of Baumgartner et al. (2012) (in agreement with inferences of Brook et al., 2000) suggest that northern sources were approximately halved during the last glacial period. The strong reduction in northern peatland emissions in LPJ-WHyMe is consistent with this inference, but it is not possible to differentiate between the boreal and subtropical northern sources using the ice-core interpolar gradient, so quantitative comparison between LPJ-WHyMe and the ice-core-based inference is difficult.

Using the transient monthly-mean GCM outputs, we have forced a series of simulations of the LPJ-WHyMe peatland and CH$_4$ emissions models. Comparisons with inferences drawn from the ice-core-derived inter-hemispheric gradient indicate that the model simulations are consistent with the newer lower values for the glacial and interstadial interpolar gradient (Baumgartner et al., 2012). Simple calculations of the atmospheric concentration changes in response to global emission increases calculated from a combination of CH$_4$ emission models (SDGVM + LPJ-WHyMe), however, significantly underpredict the overall concentration changes compared to ice-core measurements.

Comparison of the results with an independent dynamic global vegetation model (SDGVM) suggests that the model complexity of LPJ-WHyMe leads to increased sensitivity, although there are major structural differences between the models analysed, which hinders quantitative conclusions. Three modified versions of SDGVM in which the CH$_4$ module is forced with hydrological values, soil respiration

and soil temperature variables from LPJ-WHyMe were configured in order to enable a more quantitative comparison. For the abrupt warming relative to the EQ, LPJ-WHyMe was, in terms of CH$_4$ emissions, up to 8 times more sensitive than the SDGVM-LPJ-h model and up to 4 times more sensitive than the SDGVM-LPJ-hR$_h$ model. This analysis indicated that the carbon substrate in LPJ-WHyMe is more sensitive to the imposed climate, most likely due to the influence of soil freezing on plant moisture availability, whilst hydrological differences between LPJ-WHyMe and SDGVM were less important. Inclusion of the influence of soil freezing on the carbon substrate supply (by taking heterotrophic respiration from LPJ-WHyMe in the SDGVM-LPJ-hR$_h$ model) was mostly able to reproduce the base (EQ) emissions in different time periods. However, it appears that the dependence of CH$_4$ emissions on the dynamic position of the active layer is crucial for fully resolving the magnitude of the transient changes in emissions in these simulations.

A weak CH$_4$ response to abrupt AMOC variations has also been found in prior work using SDGVM and ORCHIDEE models forced with FAMOUS climate output (Hopcroft et al., 2011; Ringeval et al., 2013), and in a newer version of LPJ-WHyMe forced with a freshwater scenario under modern climatic conditions using a different model, CSM1.4 (Zürcher et al., 2013). A recent model intercomparison (Melton et al., 2013) quantified the sensitivities of 10 CH$_4$ emissions models including LPJ-WHyMe, SDGVM and ORCHIDEE. This showed that current models span a range of sensitivities to temperature, precipitation and atmospheric CO$_2$. Examining the extratropical response to a uniform temperature and precipitation increase of 3.4 °C and 3.9 % respectively, these three models span the range from −26 to +24 % change in response to warming (ORCHIDEE and LPJ-WHyMe respectively) and from 3 to 10 % change in response to precipitation increase (SDGVM and OR-CHIDEE, respectively). Together this suggests that the main conclusions reached here may be robust, but that inter-model differences are still large and require further investigation.

An important consideration for comparing emissions and concentrations of CH$_4$ is the change in atmospheric lifetime, which is largely controlled by the atmospheric burden of OH. OH concentrations are controlled directly by atmospheric temperatures and mixing and indirectly through the emissions of volatile organic compounds from vegetation. Two recent studies with 3-D atmospheric chemistry-transport simulations suggested that the combined impact of these two effects leads to a negligible change in CH$_4$ lifetime both for the G–IG transition and for abrupt climate events (Levine et al., 2011, 2012).

Other potentially relevant CH$_4$ sources not addressed in this work include biomass burning, thaw lakes and the oceans. Whilst records of charcoal suggest a dynamic relationship between climate and biomass burning (Daniau et al., 2010), ice-core isotopic evidence appears to argue against substantial contributions on either the glacial–interglacial or abrupt timescales (Möller et al., 2013). For the abrupt CH$_4$ rise at the end of the Younger Dryas, Melton et al. (2012) inferred a strong contribution from biomass burning and thaw lakes. Thaw lakes are a large source of uncertainty as they are difficult to represent realistically in global-scale models. Controversy remains over whether geological evidence signifies a rapid expansion of thaw lakes during the abrupt CH$_4$ increase at the end of the Younger Dryas (Walter et al., 2007; Reyes and Cooke, 2011), and further work is required to establish the magnitude and sensitivity of thaw lake emissions under atmospheric warming scenarios. Evidence for methanogenic bacterial communities in subglacial environments suggests a subglacial source of CH$_4$ (Wadham et al., 2008). The potential influence of subglacial environments on atmospheric CH$_4$ or on carbon substrate supply subsequent to deglaciation is uncertain.

A primary limitation in the current study is the prescription of peatland areas within the LPJ-WHyMe model. We have attempted to address this uncertainty by analysing the signals from four different distributions for each time period, but stronger palaeo-time-constraints on peatland areas would be invaluable. Another approach could rely on reconstructions of ice-sheet areas through time, adding peat areas as a function of time since deglaciation. Information on the area of glaciation for times prior to the Last Glacial Maximum is very limited due to the destruction of landscape markers by the expanding ice sheets. An alternative approach would involve predicting the accumulation of peat as a function of environmental controls (e.g. Frolking et al., 2010; Kleinen et al., 2012; Spahni et al., 2013).

6 Conclusions

Results from these simulations with a coupled atmosphere–ocean GCM and two ecosystem CH$_4$ emissions models (SDGVM and LPJ-WHyMe) suggest that changes in the Atlantic meridional overturning circulation are unlikely to be able to explain abrupt changes in atmospheric CH$_4$ as reconstructed from ice cores fully. Inclusion of peatland and permafrost physics and carbon cycling does not change this conclusion compared with two previous studies using the SDGVM and ORCHIDEE dynamic vegetation models (Hopcroft et al., 2011; Ringeval et al., 2013, respectively). However, significant changes in wetlands at lower latitudes could be important, and the incorporation of processes such as peatland development (Spahni et al., 2013) or horizontal hydrological flow (Fan and Miguez-Macho, 2011) could provide new insight.

The weak peatland source changes are consistent with new interpolar gradient data, but the total emission increases underestimate the measured changes in atmospheric concentration. Relative to a more generalised wetland scheme (such as SDGVM), the inclusion of peatland and permafrost processes in the LPJ-WHyMe model increases the climatic

sensitivity of CH$_4$ emissions. This increased sensitivity in the peatland model under equilibrium conditions is mostly due to differences in the carbon cycle productivity, whilst the increased sensitivity to abrupt warming is also partly due to the effects of freezing on soil thermodynamics. The higher sensitivity in LPJ-WHyMe however implies low simulated baseline emissions in each of the glacial time periods. This means that the rapid changes in CH$_4$ emissions are of similar magnitude in the peatland model as in the generalised wetland scheme. The variability in the magnitude of the abrupt CH$_4$ rises inferred from the ice-core record is also not convincingly replicated in the model, and this could be related to some feature of the climate scenarios used.

The CH$_4$ changes during D–O events are extremely large when compared with natural contemporary variations, and thus constitute important targets for improved understanding of the global CH$_4$ cycle. Changes in wetland emissions during these events have been inferred to be relatively strong, and modelling efforts should focus on how different wetland process representations (Ringeval et al., 2013) and mechanisms of climate change might be important for understanding D–O events. Recent studies have highlighted potential alternative mechanisms for abrupt warming aside from changes in the AMOC (Seager and Battisti, 2007; Clement and Peterson, 2008; Petersen et al., 2013), but relatively few of these have been pursued in appropriate climate modelling frameworks (Wunsch, 2006; Seager and Battisti, 2007). Future research could seek to diversify beyond freshwater the range of perturbations imposed on coupled GCMs in this context, particularly as this could lead to different patterns of climate change and hence CH$_4$ emissions.

References

Baumgartner, M., Schilt, A., Eicher, O., Schmitt, J., Schwander, J., Spahni, R., Fischer, H., and Stocker, T. F.: High-resolution interpolar difference of atmospheric methane around the Last Glacial Maximum, Biogeosciences, 9, 3961–3977, doi:10.5194/bg-9-3961-2012, 2012.

Beerling, D. J. and Woodward, F. I.: Vegetation and the Terrestrial Carbon Cycle: Modelling the first 400 Million Years, Cambridge University Press, Cambridge, 2001.

Berger, A. and Loutre, M.: Insolation values for the climate of the last 10 million years, Quaternary Sci. Rev., 10, 297–317, 1991.

Blunier, T. and Brook, E.: Timing of Millennial-Scale Climate Change in Antarctica and Greenland During the Last Glacial Period, Science, 291, 109–112, 2001.

Brook, E. J., Harder, S., Severinghaus, J., Steig, E. J., and Sucher, C. M.: On the origin and timing of rapid changes in atmospheric methane during the last glacial period, Global Biogeochem. Cy., 14, 559–572, 2000.

Cao, M., Marshall, S., and Gregson, K.: Global carbon exchange and methane emissions from natural wetlands: Application of a process-based model, J. Geophys. Res., 101, 14399–14414, 1996.

Chen, Y.-H. and Prinn, R.: Estimation of atmospheric methane emissions between 1996 and 2001 using a three-dimensional global chemical transport model, J. Geophys. Res., 111, D10307, doi:10.1029/2005JD006058, 2006.

Clement, A. and Peterson, L.: Mechanisms of Abrupt Climate Change of the Last Glacial Period, Rev. Geophys., 46, RG4002, doi:10.1029/2006RG000204, 2008.

Dällenbach, A., Blunier, T., Flückiger, J., Stauffer, B., Chappellaz, J., and Raynaud, D.: Changes in the atmospheric CH$_4$ gradient between Greenland and Antarctica during the Last Glacial and the transition to the Holocene, Geophys. Res. Lett., 27, 1005–1008, 2000.

Daniau, A.-L., Harrison, S., and Bartlein, P.: Fire regimes during the Last Glacial, Quaternary Sci. Rev., 29, 2918–2930, 2010.

Elliot, M., Labeyrie, L., and Duplessy, J.-C.: Changes in North Atlantic deep-water formation associated with the Dansgaard–Oeschger temperature oscillations (60–10 ka), Quaternary Sci. Rev., 21, 1153–1165, doi:10.1016/S0277-3791(01)00137-8, 2002.

Fan, Y. and Miguez-Macho, G.: A simple hydrologic framework for simulating wetlands in climate and earth system models, Clim. Dynam., 37, 253–278, doi:10.1007/s00382-010-0829-8, 2011.

Flückiger, J., Blunier, T., Stauffer, B., Chappellaz, J., Spahni, R., Kawamura, K., Schwander, J., Stocker, T. F., and Dahl-Jensen, D.: N$_2$O and CH$_4$ variations during the last glacial epoch: Insight into global processes, Global Biogeochem. Cy., 18, GB1020, doi:10.1029/2003GB002122, 2004.

Frolking, S., Roulet, N. T., Tuittila, E., Bubier, J. L., Quillet, A., Talbot, J., and Richard, P. J. H.: A new model of Holocene peatland net primary production, decomposition, water balance, and peat accumulation, Earth Syst. Dynam., 1, 1–21, doi:10.5194/esd-1-1-2010, 2010.

Ganopolski, A. and Rahmstorf, S.: Rapid changes of glacial climate simulated in a coupled climate model, Nature, 409, 153–155, 2001.

Gerten, D., Schaphoff, S., Haberlandt, U., Lucht, W., and Sitch, S.: Terrestrial vegetation and water balance: Hydrological evaluation of a dynamic global vegetation model, J. Hydrol., 286, 249–270, 2004.

Gherardi, J.-M., Labeyrie, L., McManus, J. F., Francois, R., Skinner, L. C., and Cortijo, E.: Evidence from the northeastern atlantic basin for variability in the rate of the meridional overturning circulation through the last deglaciation, Earth Planet. Sc. Lett., 240, 710–723, 2005.

Gordon, C., Cooper, C., Senior, C. A., Banks, H., Gregory, J. M., Johns, T. C., Mitchell, J. F. B., and Wood, R. A.: The simulation of sst, sea ice extents and ocean heat transports in a version of the Hadley Centre coupled model without flux adjustments, Clim. Dynam., 16, 147–168, 2000.

Granberg, G., Grip, H., Ottosson Löfvenius, M., Sundh, I., Svensson, B. H., and Nilsson, M.: A simple model for simulation of water content, soil frost, and soil temperatures in boreal mixed mires, Water Resour. Res., 35, 3771–3782, 1999.

Halsey, L., Vitt, D., and Gignac, L.: phSphagnum-dominated Peatlands in North America Since the Last Glacial Maximum: Their Occurrence and Extent, Bryologist, 103, 334–352, 2000.

Harrison, S. and Sanchez-Goñi, M.: Global patterns of vegetation response to millennial-scale variability and rapid climate change during the last glacial period, Quaternary Sci. Rev., 29, 21–22, 2957–2980, 2010.

Hendy, I. and Kennett, J.: Dansgaard–Oeschger cycles and the California Current System: Planktonic foraminiferal response to rapid climate change in Santa Barbara Basin, Ocean Drilling Program hole 893A, Paleoceanography, 15, 30–42, 2000.

Hopcroft, P., Valdes, P., and Beerling, D.: Simulating idealized Dansgaard–Oeschger events and their potential impacts on the global methane cycle, Quaternary Sci. Rev., 30, 3258–3268, 2011.

Huber, C., Leuenberger, M., Spahni, R., Flückiger, J., Schwander, J., Stocker, T., Johnsen, S., Landais, A., and Jouzel, J.: Isotope calibrated Greenland temperature record over Marine Isotope Stage 3 and its relation to CH₄, Earth Planet. Sc. Lett., 243, 504–519, 2006.

Kanner, L. C., Burns, S. J., Cheng, H., and Edwards, R. L.: High-Latitude Forcing of the South American Summer Monsoon During the Last Glacial, Science, 335, 570–573, 2012.

Kleinen, T., Brovkin, V., and Schuldt, R. J.: A dynamic model of wetland extent and peat accumulation: results for the Holocene, Biogeosciences, 9, 235–248, doi:10.5194/bg-9-235-2012, 2012.

Korhola, A., Ruppel, M., Seppä, H., Väliranta, M., Virtanen, T., and Weckström, J.: The importance of northern peatland expansion to the late-Holocene rise of atmospheric methane, Quaternary Sci. Rev., 29, 611–617, 2009.

Levine, J., Wolff, E., Jones, A., Sime, L., Valdes, P., Archibald, A., Carver, G., Warwick, N., and Pyle, J.: Reconciling the changes in atmospheric methane sources and sinks between the Last Glacial Maximum and the pre-industrial era, Geophys. Res. Lett., 38, L23804, doi:10.1029/2011GL049545, 2011.

Levine, J., Wolff, E., Hopcroft, P., and Valdes, P.: Controls on the tropospheric oxidising capacity during an idealized Dansgaard–Oeschger event, and their implications for the rapid rises in atmospheric methane during the last glacial period, Geophys. Res. Lett., 39, L12805, doi:10.1029/2012GL051866, 2012.

Li, C., Battisti, D., and Bitz, C.: Can North Atlantic Sea Ice Anomalies Account for Dansgaard–Oeschger Climate Signals?, J. Climate, 23, 5457–5475, 2010.

Liu, Z., Otto-Bleisner, B., H. F., Brady, E., Tomas, R., Clark, P., Carlson, A., Lynch-Steiglitz, J., Curry, W., Brook, E., Erickson, D., Jacob, R., Kutzbach, J., and Cheng, J.: Transient Simulation of Last Deglaciation with a New Mechanism for Bølling-Allerød Warming, Science, 325, 310–314, 2009.

MacDonald, G. M., Beilman, D. W., Kremenetski, K. V., Sheng, Y., Smith, L. C., and Velichko, A. A.: Rapid Early Development of Circumarctic Peatlands and Atmospheric CH₄ and CO₂ Variations, Science, 314, 285–288, 2006.

Masson-Delmotte, V., Jouzel, J., Landais, A., Stievenard, M., Johnsen, S. J., White, J. W. C., Sveinbjornsdottir, A., and Fuhrer, K.: Deuterium excess reveals millennial and orbital scale fluctuations of Greenland moisture origin, Science, 309, 118–121, 2005.

Melton, J. R., Schaefer, H., and Whiticar, M. J.: Enrichment in ¹³C of atmospheric CH₄ during the Younger Dryas termination, Clim. Past, 8, 1177–1197, doi:10.5194/cp-8-1177-2012, 2012.

Melton, J. R., Wania, R., Hodson, E. L., Poulter, B., Ringeval, B., Spahni, R., Bohn, T., Avis, C. A., Beerling, D. J., Chen, G., Eliseev, A. V., Denisov, S. N., Hopcroft, P. O., Lettenmaier, D. P., Riley, W. J., Singarayer, J. S., Subin, Z. M., Tian, H., Zürcher, S., Brovkin, V., van Bodegom, P. M., Kleinen, T., Yu, Z. C., and Kaplan, J. O.: Present state of global wetland extent and wetland methane modelling: conclusions from a model intercomparison project (WETCHIMP), Biogeosciences, 10, 753–788, doi:10.5194/bg-10-753-2013, 2013.

Merkel, U., Prange, M., and Schulz, M.: ENSO variability and teleconnections during glacial climates, Quaternary Sci. Rev., 29, 86–100, 2010.

Möller, L., Sowers, T., Bock, M., Spahni, R., Behrens, M., Schmitt, J., Miller, H. and Fischer, H.: Independent variations of CH₄ emissions and isotopic composition over the past 160,000 years, Nat. Geosci., 6, 885–890, 2013.

New, M., M. Hulme, and P. D. Jones: Representing twentieth century space-time climate variability, Part 1: Development of a 1961–1990 mean monthly terrestrial climatology, J. Climate, 12, 829–856, 1999.

NGRIP Project Members: High-resolution record of Northern Hemisphere climate extending into the last interglacial period, Nature, 431, 47–151,, 2004.

Pausata, F., Battisti, D., Nisancioglu, K., and Bitz, C.: Chinese stalagmite δ¹⁸O controlled by changes in the Indian monsoon during a simulated Heinrich event, Nat. Geosci., 4, 474–480, 2011.

Peltier, W.: Global glacial isostasy and the surface of the ice age earth: The ICE-5G (VM2) model and GRACE, Annu. Rev. Earth Planet. Sci., 32, 111–149, 2004.

Petersen, S., Schrag, D., and Clark, P.: A new mechanism for Dansgaard–Oeschger cycles, Paleoceanography, 28, 24–30, 2013.

Peterson, L. C., Haug, G. H., Hughen, K. A., and Rohl, U.: Rapid changes in the hydrologic cycle of the tropical Atlantic during the last glacial, Science, 290, 1947–1951, 2000.

Petit, J. R., Jouzel, J., Raynaud, D., Barkov, N. I., Barnola, J.-M., Basile, I., Bender, M., Chappellaz, J., Davis, M., Dalaygue, G., Delmotte, M., Kotlyakov, V. M., Legrand, M., Lipenkov, V. Y., Lorius, C., Pépin, L., Ritz, C., Saltzman, E., and Stievenard, M.: Climate and atmospheric history of the past 420,000 years from the Vostok Ice Core, Antarctica, Nature, 399, 429–436, 1999.

Reyes, A. and Cooke, C.: Northern peatland initiation lagged abrupt increases in deglacial atmospheric CH₄, P. Natl. Acad. Sci., 108, 4748–4753, 2011.

Ringeval, B., Hopcroft, P. O., Valdes, P. J., Ciais, P., Ramstein, G., Dolman, A. J., and Kageyama, M.: Response of methane emissions from wetlands to the Last Glacial Maximum and an idealized Dansgaard–Oeschger climate event: insights from two models of different complexity, Clim. Past, 9, 149–171, doi:10.5194/cp-9-149-2013, 2013.

Seager, R. and Battisti, D. S.: Challenges to our understanding of the general circulation: abrupt climate change, in: The Global Circulation of the Atmosphere, edited by: Lorenz, E. N., Schneider, T., and Sobel, A. H., Princeton University Press, Princeton, USA, 2007.

Singarayer, J. and Valdes, P.: High-latitude climate sensitivity to ice-sheet forcing over the last 120 kyr, Quaternary Sci. Rev., 29, 43–55, 2010.

Singarayer, J., Valdes, P., Friedlingstein, P., Nelson, S., and Beerling, D.: Late Holocene methane rise caused by orbitally controlled increase in tropical sources, Nature, 470, 82–85, 2011.

Smith, R. S., Gregory, J. M., and Osprey, A.: A description of the FAMOUS (version XDBUA) climate model and control run, Geosci. Model Dev., 1, 53–68, doi:10.5194/gmd-1-53-2008, 2008.

Spahni, R., Chappellaz, J., Stocker, T. F., Loulergue, L., Hausammann, G., Kawamura, K., Flückiger, J., Schwander, J., Raynaud, D., Masson-Delmotte, V., and Jouzel, J.: Atmospheric methane and nitrous oxide of the late pleistocene from Antarctic ice cores, Science, 310, 1317–1321, 2005.

Spahni, R., Wania, R., Neef, L., van Weele, M., Pison, I., Bousquet, P., Frankenberg, C., Foster, P. N., Joos, F., Prentice, I. C., and van Velthoven, P.: Constraining g lobal methane emissions and uptake by ecosystems, Biogeosciences, 8, 1643-1665, doi:10.5194/bg-8-1643-2011, 2011.

Spahni, R., Joos, F., Stocker, B. D., Steinacher, M., and Yu, Z. C.: Transient simulations of the carbon and nitrogen dynamics in northern peatlands: from the Last Glacial Maximum to the 21st century, Clim. Past, 9, 1287–1308, doi:10.5194/cp-9-1287-2013, 2013.

Talley, L., Reid, J., and Robbins, P.: Data-based Meridional Overturning Streamfunctions for the Global Ocean, J Climate, 16, 3213–3226, 2003.

Valdes, P., Beerling, D., and Johnson, C.: The ice age methane budget, Geophys. Res. Lett., 32, L02704, doi:10.1029/2004GL021004, 2005.

van Huissteden, J.: Methane emission from northern wetlands in Europe during Oxygen Isotope Stage 3, Quaternary Sci. Rev., 23, 1989–2005, 2004.

van Kreveld, S., Sarnthein, M., Erlenkeuser, H., Grootes, P., Jung, S., Nadeau, M. J., Pflaumann, U., and Voelker, A.: Potential links between surging ice sheets, circulation changes, and the Dansgaard–Oeschger cycles in the Irminger Sea, 60–18 kyr, Paleoceanography, 15, 425–442, 2000.

Wadham, J., Tranter, M., Tulaczyk, S., and Sharp, M.: Subglacial methanogenesis: A potential climatic amplifier?, Global Biogeochem. Cy., 22, GB2021, doi:10.1029/2007GB002951, 2008.

Walter, K. M., Edwards, M. E., Grosse, G., Zimov, S. A., and Chapin III, F. S.: Thermokarst Lakes as a Source of Atmospheric CH$_4$ During the Last Deglaciation, Science, 318, 633–636, 2007.

Wang, Y. J., Cheng, H., Edwards, R. L., An, Z. S., Wu, J. Y., Shen, C.-C., and Dorale, J. A.: A High-Resolution Absolute-Dated Late Pleistocene Monsoon Record from Hulu Cave, China, Science, 24, 2345–2348, 2001.

Wania, R., Ross, I., and Prentice, I. C.: Integrating peatlands and permafrost into a dynamic global vegetation model: 1. evaluation and sensitivity of physical land surface processes, Global Biogeochem. Cy., 23, GB3014, doi:10.1029/2008GB003412, 2009a.

Wania, R., Ross, I., and Prentice, I. C.: Integrating peatlands and permafrost into a dynamic global vegetation model: 2. evaluation and sensitivity of vegetation and carbon cycle processes, Global Biogeochem. Cy., 23, GB3015, doi:10.1029/2008GB003413, 2009b.

Wania, R., Ross, I., and Prentice, I. C.: Implementation and evaluation of a new methane model within a dynamic global vegetation model: LPJ-WHyMe v1.3.1, Geosci. Model Dev., 3, 565–584, doi:10.5194/gmd-3-565-2010, 2010.

Wania, R., Melton, J. R., Hodson, E. L., Poulter, B., Ringeval, B., Spahni, R., Bohn, T., Avis, C. A., Chen, G., Eliseev, A. V., Hopcroft, P. O., Riley, W. J., Subin, Z. M., Tian, H., van Bodegom, P. M., Kleinen, T., Yu, Z. C., Singarayer, J. S., Zürcher, S., Lettenmaier, D. P., Beerling, D. J., Denisov, S. N., Prigent, C., Papa, F., and Kaplan, J. O.: Present state of global wetland extent and wetland methane modelling: methodology of a model inter-comparison project (WETCHIMP), Geosci. Model Dev., 6, 617–641, doi:10.5194/gmd-6-617-2013, 2013.

Whiting, G. and Chanton, J.: Primary production control of methane emission from wetlands, Nature, 364, 794–795, 1993.

Wolff, E. W., Chappellaz, J., Blunier, T., Rasmussen, S. O., and Svensson, A.: Millennial-scale variability during the last glacial: The ice core record, Quaternary Sci. Rev., 29, 2828–2838, 2010.

Woodward, F., Smith, T., and Emanuel, W.: A global land primary productivity and phytogeography model, Global Biogechem. Cy., 9, 471–490, 1995.

Wunsch, C.: Abrupt climate change: An alternative view, Quaternary Sci. Rev., 65, 191–203, 2006.

Yin, J., Schlesinger, M., Andronova, N., Malyshev, S., and Li, B.: Is a shutdown of the thermohaline circulation irreversible?, J. Geophys. Res., 11, D12104, doi:10.1029/2005JD006562, 2006.

Yu, Z., Loisel, J., Brosseau, D., and Beilman, D.: Global peatland dynamics since the Last Glacial Maximum, Geophys. Res. Lett., 37, L13402, doi:10.1029/2010GL043584, 2010.

Zürcher, S., Spahni, R., Joos, F., Steinacher, M., and Fischer, H.: Impact of an abrupt cooling event on interglacial methane emissions in northern peatlands, Biogeosciences, 10, 1963–1981, doi:10.5194/bg-10-1963-2013, 2013.